



1 Impact of Siberia forest fires on the atmospheric environment over the
2 Korean Peninsula during summer 2014

3

4 Jinsang Jung ^{a,*}, Youngsook Lyu^b, Minhee Lee^b, Taekyung Hwang^b, Youdeok Hong^b,
5 Jihyung Hong^b, Sangil Lee^a, Sanghyub Oh^a

6

7 ^aCenter for Gas Analysis, Korea Research Institute of Standards and Science (KRISS),
8 Daejeon 34113, Republic of Korea

9 ^bDepartment of Climate and Air Quality Research, National Institute of Environmental
10 Research, Daejeon 34944, Republic of Korea

11

12

13 Running title: LRT Russian FF

14

15 Last modified: January 19, 2015

16 Submitted to Atmospheric Chemistry and Physics

17

18 *Corresponding author: Jinsang Jung (jsjung@kriss.re.kr)

19

20 **Abstract**

21 Extensive forest fires occurred during the late July, 2014 across the Siberia forest
22 region, Russia. Smoke plumes emitted from the Siberia forest fires were long-range
23 transported through Mongolia and northeast China, and down to the Korean Peninsula,
24 which is located at ~3,000 km south of the Siberia forest. Notably high aerosol optical
25 depth (AOD) of ~4 was observed at a wavelength of 500 nm near the source region of
26 the Siberia forest fires. The smoke plumes reached about 3–5 km height near the source
27 region and then below 2 km height near the Korean Peninsula. Elevated concentration
28 of levoglucosan was observed as an average of $119.7 \pm 6.0 \text{ ng m}^{-3}$ (mean \pm one standard
29 deviation) which was ~4.5 times higher than those observed during the non-event period
30 in July, 2014. During the middle of July 2014, another type of haze episode occurred
31 that was mainly caused by long-range transported haze plumes originated from urban
32 and industrial complexes in the East China. Sharp increases in SO_4^{2-} concentrations
33 ($23.1 \pm 2.1 \mu\text{g m}^{-3}$) were observed during the Chinese haze episode. The haze episode
34 caused by the long-range transported Siberia forest fires was clearly distinguished with
35 relatively high OC/EC ratio (7.18 ± 0.2) and OC/ SO_4^{2-} ratio (1.31 ± 0.07) compared to
36 those (OC/EC ratio: 2.4 ± 0.4 , OC/ SO_4^{2-} ratio: 0.21 ± 0.05) during the Chinese haze
37 episode. Remote measurement techniques and chemical analyses of the haze plumes
38 clearly showed that the haze episode occurred during the late July, 2014 was mainly
39 caused by the long-range transported smoke plumes emitted from Siberia forest fires.

40



41 1. Introduction

42 Forest fires emit large amounts of gaseous and particulate pollutants into the
43 atmosphere, namely carbon dioxide (CO₂), carbon monoxide (CO), methane (CH₄),
44 nitrogen oxides (NO_x), ammonia (NH₃), particulate matter (PM), non-methane
45 hydrocarbon (NMHC), and other chemical species (Crutzen and Andreae, 1990). These
46 gaseous and particulate pollutants can alter regional climate in downwind area by
47 altering ambient temperature, cloud property and the efficiency of precipitation (Jeong
48 et al., 2008; Youn et al., 2011; Jeong et al., 2014). They can also influence the air quality
49 of downwind areas in urban, ocean, and Arctic regions through long-range atmospheric
50 transport (Carvalho et al., 2011; Quennehe et al., 2012; Schreier et al., 2015).

51 During the severe forest fires smoke episode in Moscow, Russia in August 2010,
52 notably high concentrations of total carbon (average 202 μg m⁻³) and levoglucosan (3.1
53 μg m⁻³) were observed with elevated organic carbon/elemental carbon (OC/EC) ratio of
54 27.4 (Popovicheva et al., 2014). Total carbon concentration during the severe smoke
55 episode exceeded 10 times that during the non-event period in Moscow, Russia
56 (Popovicheva et al., 2014). During the severe forest fires smoke episode in Siberia
57 region in May 2003, the surface PM₁₀ and O₃ concentrations in the downwind areas
58 increased by 5–30 μg m⁻³ and 3–20 ppbv, respectively, having an important implication
59 for air quality over East Asia (Jeong et al., 2008).

60 The territory of Russian Federation is covered with over 800 million hectares of
61 forest, which is equal to 50 billion tons of growing carbon stock, where annually about
62 1% is damaged by fires (Bondur, 2010; Popovicheva et al., 2014). Russian boreal
63 forests are subject to frequent wildfires. Each year, 10–35 thousand forest fires covering
64 5,000–53,000 km² (including 4,000–10,000 km² of high intensity, stand-replacing fires)



65 were detected in actively protected portions of the Russian forest (Bartalev et al., 1977;
66 Isaev et al., 2002; Mei et al., 2011). Siberia is one of the world's major boreal forest fire
67 areas as approximately 12,000–34,000 wildfires occurred every year in Russia for the
68 period 1974–1993 (Conard and Eduard, 1996).

69 Frequent forest fires over the Siberia region had an impact on downwind areas in
70 Mongolia, China, Korea and Northwestern Pacific through long-range atmospheric
71 transport (Kajii et al., 2002; Kanaya et al., 2003; Lee et al., 2005; Jeong et al., 2008;
72 Youn et al., 2011). In May 2003, intense forest fires occurred over Siberia (Lee et al.,
73 2005; Jeong et al., 2008; Youn et al., 2011). Satellite observation clearly showed the
74 transport of the smoke plume emitted from the Siberia forest fires through Mongolia
75 and eastern China, down to the Korean Peninsula (Lee et al., 2005). Simulation results
76 by Youn et al. (2011) showed a significant surface cooling of -3.5 K over Siberia forest
77 region. The simulation also showed that smoke aerosols affected the large-scale
78 circulations and resulted in the increases in rainfall rates of 2.9 mm day⁻¹ averaged over
79 the northern west Pacific. Jeong et al. (2008) reported that the smoke plume from the
80 Siberian forest fires in May 2003 acts mainly as a cooling agent, resulting in a negative
81 radiative forcing of -5.8 Wm⁻² at the surface over East Asia.

82 Severe wildfires occurred in the Russian forest region during summer, 2014.
83 Intensity of wildfires during the summer, 2014 appears to be three times bigger than
84 2013. According to NASA MODIS FIRMS (Fire Information for Resource Management
85 System), daily average of ~5,000 active fires were detected in the Siberia forest region
86 covering Irkutsk to Yakutsk area during 15–25 July 2014
87 (<https://earthdata.nasa.gov/active-fire-data-tab-content-6>). MODIS satellite RGB images



88 clearly showed that these smoke plumes lasted more than a week and transported
89 southern direction down to Mongolia, northern China and the Korean Peninsula.

90 In this study, we investigate the smoke plumes emitted from Siberia forest fires
91 during the late July, 2014 and their long-range atmospheric transport to the Korean
92 Peninsula. Spatial transport mechanism of the smoke plumes is investigated based on
93 satellite image analyses and satellite-based lidar observation. We also characterize the
94 chemical composition of the long-range transported smoke plumes reached at the
95 Korean Peninsula. In contrast to the forest fire plume event, chemical characteristics of
96 long-range transported anthropogenic pollutants from East China are also investigated.

97

98 2. Experimental Methods

99 2.1 Atmospheric aerosol sampling and sample preparation

100 Daily $PM_{2.5}$ (particulate matter with a diameter less than or equal to 2.5 micrometers)
101 sampling was carried out at a central region air quality monitoring station (36.19 °N,
102 127.24 °E) in Daejeon, Korea from 1 to 31 July 2014. $PM_{2.5}$ samples were collected on
103 pre-baked quartz fiber filters (Pall-Life Sciences, 47 mm diameter) using an aerosol
104 sampler (APM Korea, model PMS-103) at a flow rate of 16.7 L min⁻¹ on the rooftop of
105 a comprehensive monitoring building (~15 m above the ground) of National Institute of
106 Environmental Research in Korea. Before and after sampling, the filter samples were
107 stored in a freezer wrapped with aluminum foil at -20 °C. A total of 31 filter samples
108 were collected in this study, and additional field blank filters were collected before and
109 after the sampling period.

110 Ultrapure water used in this study was prepared using a Labpure S1 filter and a
111 ultra-violet (UV) lamp (ELGA, PureLab Ultra). Resistivity and total organic carbon



112 (TOC) values of the ultrapure water were maintained as $18.2 \text{ M}\Omega \text{ cm}^{-1}$ and 4 ppb,
113 respectively. To measure carbohydrates and water-soluble ions, a quarter of each filter
114 sample was extracted with 10 mL of ultrapure water under ultrasonication (for 30 min)
115 and then passed through a disk filter (Millipore, Millex-GV, 0.45 mm). Water extracts
116 were stored in a refrigerator at 4 °C before analysis.

117

118 2.2 Analysis of chemical composition of fine particles

119 Mass concentration of $\text{PM}_{2.5}$ was measured using a beta-attenuation technique (Met
120 One Instruments, BAM 1020), with an hourly averaging time resolution. The detection
121 limit and measurement error of the beta-attenuation technique were reported as $3.6 \mu\text{g}$
122 m^{-3} and 8 %, respectively by the manufacturer. In addition to $\text{PM}_{2.5}$ mass concentration,
123 chemical composition of daily $\text{PM}_{2.5}$ was also characterized through filter sampling and
124 laboratory analysis. Because the time interval of chemical composition of $\text{PM}_{2.5}$ was
125 daily basis, daily average $\text{PM}_{2.5}$ mass data was calculated from average $\text{PM}_{2.5}$ mass data
126 and used in this study.

127

128 2.2.1 Levoglucosan and mannosan analysis

129 Levoglucosan and mannosan were analyzed by an improved high-performance
130 anion-exchange chromatography (HPAEC) method with pulsed amperometric detection
131 (PAD) (Engling et al., 2006; Jung et al., 2014). The HPAEC-PAD system uses an ion
132 chromatograph consisting of an electrochemical detector and gold electrode unit, along
133 with an AS40 auto-sampler (Thermo Fisher Scientific, Dionex ICS-15000).
134 Levoglucosan and mannosan were separated by a CarboPak MA1 analytical column (4
135 x 250 mm) and a sodium hydroxide solution as an eluent. The detection limit of



136 levoglucosan and mannosan was 3.0 and 0.7 ng m^{-3} , respectively. The analytical error,
137 defined as the ratio of the standard deviation to the average value, obtained from
138 triplicate analyses of filter samples, was 1.9% and 0.73%, for levoglucosan and
139 mannosan, respectively.

140

141 2.2.2 Water-soluble inorganic ions analysis

142 Water-soluble inorganic ions were analyzed using an ion chromatography (Thermo
143 Fisher Scientific, Dionex ICS-15000). The anions; nitrate (NO_3^-) and sulfate (SO_4^{2-}),
144 were separated using an IonPAC AS15 column with an eluent of 20 mM of potassium
145 hydroxide (KOH) at flow rate of 0.5 mL min^{-1} . The detection limits of NO_3^- and SO_4^{2-} ,
146 which are defined as 3 times standard deviation of field blanks, were 0.01 and $0.11 \text{ }\mu\text{g}$
147 m^{-3} , respectively. The analytical errors of NO_3^- and SO_4^{2-} were 2.3% and 1.7%,
148 respectively. The cations, sodium (Na^+), ammonium (NH_4^+), potassium (K^+),
149 calcium (Ca^{2+}), and magnesium (Mg^{2+}), were separated using an IonPac CS-12A column
150 ($4 \times 250 \text{ mm}$) with an eluent of 38 mM of methanesulfonic acid (MSA) at a flow rate of
151 1.0 mL min^{-1} . The detection limits of NH_4^+ and K^+ were 0.03 and $0.006 \text{ }\mu\text{g m}^{-3}$,
152 respectively. The analytical errors of NH_4^+ and K^+ were 1.4% and 0.73%, respectively.

153

154 2.2.3 Organic carbon/elemental carbon analysis

155 $\text{PM}_{2.5}$ carbonaceous aerosol was measured using a semi-continuous organic
156 carbon/elemental carbon (OC/EC) analyzer (Sunset Lab., Model RT3140). The air
157 samples were drawn at 8 L min^{-1} through a $\text{PM}_{2.5}$ sharp-cut cyclone. The sampled
158 aerosols then were passed through a multichannel parallel plate denuder with a carbon-
159 impregnated filter to remove semi-volatile organic vapors, and then collected on a



160 quartz-fiber filter. The sampled aerosols were analyzed based on thermal-optical
161 transmittance (TOT) protocol for pyrolysis correction and NIOSH (National Institute
162 for Occupational Safety and Health) 5040 method temperature profile (Birch and Cary,
163 1996; Jung et al., 2010). External calibration was performed using known amounts of
164 sucrose. The detection limit of both OC and EC was $0.5 \mu\text{g C m}^{-3}$ for 1 hr time
165 resolution reported by the manufacturer. The uncertainty of OC and EC measurements
166 is reported as 5% (Polidori et al., 2006).

167

168 2.3 Satellite aerosol optical depth and air mass backward trajectories

169 The NOAA/ARL HYSPLIT (HYbrid Single-Particle Lagrangian Trajectory) air
170 mass backward trajectory analysis (Draxler and Rolph, 2015; Rolph, 2015) and
171 Moderate Resolution Imaging Spectro-radiometer (MODIS) satellite image analysis
172 were used to characterize potential source regions and the transport pathway of the haze
173 plume. Air mass backward trajectories ended at the measurement site were computed
174 for 200, 500 and 1000 m above ground level (AGL) heights using the HYSPLIT model.
175 All back-trajectories were calculated at 00:00 UTC and 12:00 UTC (09:00 LT and
176 21:00 LT, respectively) extending to 96 h backward with 1 h time interval. The
177 calculated air mass pathways indicate the general airflow pattern rather than the exact
178 pathway of air masses because the typical error of the traveled distance are up to 20%
179 for the trajectories computed from analyzed wind fields (Stohl, 1998),.

180 Aerosol optical thickness (AOT) data retrieved by the V5.2 version of the NASA
181 MODIS algorithm, called Collection 005 (C005) (Levy et al., 2007a, b) were used in
182 this study. AOT data, which is part of the MODIS Terra/Aqua Level-2 gridded
183 atmospheric data product, are available on the MODIS web site



184 (<http://modis.gsfc.nasa.gov/>). Cloud-screened Level 1.5 sunphotometer data at Yakutsk
185 site (61.66 °N, 129.37 °E, 118 m above sea level) and Ussuriysk site (43.70 °N,
186 132.16 °E, 280 m above sea level) in Russia were obtained from the AERONET site
187 (<http://aeronet.gsfc.nasa.gov>). This study used total column-integrated spectral aerosol
188 optical thickness (AOT) determined by the AERONET algorithm (Dubovik and King,
189 2000).

190 CALIOP (Cloud-Aerosol Lidar with Orthogonal Polarization) is a space based lidar
191 system onboard the Cloud Aerosol Lidar and Infrared Pathfinder Satellite Observations
192 (CALIPSO) satellite launched in 2006 (Winker et al., 2009). This study used version
193 2.30 data of total attenuated backscatter at 532 nm. Expedited CALIPSO browse images
194 were obtained from the CALIPSO website ([http://www-
195 calipso.larc.nasa.gov/products/lidar/browse_images/show_calendar.php](http://www-calipso.larc.nasa.gov/products/lidar/browse_images/show_calendar.php)).

196

197 3. Results and Discussion

198 3.1 Overview of chemical composition of fine particulate matter (PM_{2.5})

199 Figure 2 shows temporal variations of chemical compositions of PM_{2.5} at the
200 Daejeon site during the entire measurement period. Daily average PM_{2.5} mass
201 concentrations ranged from 8.0 µg m⁻³ to 65.1 µg m⁻³ with an average of 27.5 ± 15.2 µg
202 m⁻³. Two peaks of PM_{2.5} mass concentration were obtained during 12–16 July (first
203 episode) and 27–28 July 2014 (second episode). PM_{2.5} mass concentrations reached to
204 65.1 µg m⁻³ and 56.2 µg m⁻³ during the first and second episodes, respectively. The
205 temporal variation of the sum of PM_{2.5} chemical compositions showed a similar pattern
206 with that of total PM_{2.5} mass as shown in Fig. 2. During the entire measurement period,
207 SO₄²⁻ was found as the highest value with an average of 8.8 ± 7.0 µg m⁻³, followed by



208 OC ($4.3 \pm 2.0 \mu\text{g m}^{-3}$), NH_4^+ ($4.3 \pm 3.3 \mu\text{g m}^{-3}$), EC ($1.1 \pm 0.4 \mu\text{g m}^{-3}$), and NO_3^- ($1.0 \pm$
209 $1.1 \mu\text{g m}^{-3}$) with minor contributions from Ca^{2+} , K^+ , and Na^+ .

210

211 3.2 Classification of haze episodes during summer, 2014

212 3.2.1 Long-range transported smoke plumes from Siberia forest fires

213 MODIS RGB images clearly show severe smoke plumes over the Siberia forest
214 region during the late July, 2014. Figure 3a shows a typical example of satellite RGB
215 images of the smoke plumes emitted from Siberia forest fires and their atmospheric
216 transport to south during 25 July 2014. Fire events in the Siberia forest region were
217 from the MODIS active fire product (Gilio et al., 2003) and expressed as red dots in
218 Fig. 3a. It is clearly seen that the smoke plumes originated from the Siberia forest fires
219 lingered to the southern direction of the Korean Peninsula across Mongolia and
220 northeast China. HYSPLIT backward trajectory analyses in Fig. 3b also show that air
221 masses originated from the Siberia forest region transported to the Korean Peninsula
222 during 26–28 July 2014.

223 Figure 4 shows horizontal distribution of aerosol optical depth (AOD) over the East
224 Asia during 23–28 July 2014. High loading of AOD was clearly shown over the
225 Siberia forest region on 23 July when forest fires occurred. The transport of high
226 loading of AOD was clearly seen down to northeast China and further to the Korean
227 Peninsula from 23 July to 28 July 2014 (Fig. 4). These horizontal distributions of AOD
228 also support the transport of smoke plumes emitted from the Siberia forest fires into
229 the Korean Peninsula during the late July, 2014.

230 Figure 5 shows temporal variations of AODs measured by a sunphotometer at the
231 Yakutsk and Ussuriysk sites. The Yakutsk site is located near the source region of the



232 Siberia forest fires whereas the Ussuriysk site is located close to the north of the
233 Korean Peninsula as shown in Fig. 3. AOD measured at the Yakutsk site started to
234 increase from 23 July and high AOD continued until 26 July 2014. The maximum
235 AOD reached at ~4 at the Yakutsk site during 24 July 2014 when the Siberia forest
236 fires occurred. The high loading of AOD lasted for 4 days at the Yakutsk site during
237 the Siberia forest fires episodes. Interestingly, a sharp increase in AOD was also
238 observed at the Ussuriysk site during 24 July 2014. This result implied the rapid
239 transport of the smoke plumes to the northern Korean Peninsula within one day.

240 Figure 6 shows MODIS RGB images and vertical distributions of total attenuated
241 backscatter at a wavelength of 532 nm measured by the CALIPSO satellite during 24,
242 25, and 27 July 2014. Yellow and red colors in the total attenuated backscatter
243 measurement in Fig. 6 represent atmospheric aerosols whereas white color represents
244 cloud. Yellow lines over MODIS RGB images in Fig 6 represent the observation
245 routes of the CALIPSO satellite. Figure 6a and b clearly showed that smoke layer
246 existed approximately 3–5 km height near the source region of the Siberia forest fires
247 during 24 and 25 July 2014. As shown in Fig. 6c, the height of the smoke layer
248 decreased to below 2 km height during 27 July 2014 when it reached to the Korean
249 Peninsula.

250 From the spatial distribution of AOD obtained by MODIS and CALIPSO satellite
251 observations and HYSPLIT air mass backward trajectory analyses, it was clearly seen
252 that the smoke plumes originated from the Siberia forest fires during 23–24 July 2014
253 transported over 3000 km in the southerly direction and had an impact on the Korean
254 Peninsula during 27–28 July 2014. Ground based AOD measurements by a



255 sunphotometer near the Siberia forest fire area and the Korean Peninsula also supported
256 the transport of the smoke plume originated from the Siberia forest fires into the
257 Korean Peninsula. Thus, in this study, the smoke episode during 27–28 July 2014 is
258 defined as the Siberia forest fire episode.

259

260 3.2.2 Long-range transported haze under Asian continental outflow

261 Besides the haze episode caused by the long-range transported smoke plume emitted
262 from the Siberia forest fires during the late July, 2014, another haze episode was
263 observed in the Daejeon site during 14–16 July 2014 as shown in Fig. 2. From the
264 MODIS RGB image on 14 July in Fig. 7, it was clearly shown that a severe haze plume
265 originated from East China lingered to the Korean Peninsula across the Yellow Sea.
266 HYSPLIT backward air mass trajectories also showed transport of air masses originated
267 from the East China to the Korean Peninsula over the Yellow Sea during 15–16 July
268 2014.

269 The East China covering from Beijing to Shanghai region consists of heavily
270 populated, urbanized, and industrialized cities (Chan and Yao, 2008). Thus, a large
271 amount of anthropogenic pollutants is emitted from these regions in the East China (Li
272 et al., in press). Figure 8 shows horizontal distribution of MODIS AOD over East Asia
273 during 13–16 July 2014. It is clearly seen that the high loading of AOD over East China
274 lingered to the Korean Peninsula over the Yellow Sea. These results suggest that the
275 haze episode during 14–16 July 2014 was mainly originated from long-range transport
276 of pollutants originated from the East China. Thus, in this study, the haze episode
277 during 14–16 July is defined as the Chinese haze episode.

278



279 3.3 Chemical characterization of the long-range transported haze plumes

280 3.3.1 Comparison of PM_{2.5} chemical composition during the haze episodes

281 Figure 9 shows temporal variations of PM_{2.5} mass concentration and its selected
282 chemical components. During the Chinese haze episode, elevated concentrations of
283 SO₄²⁻ (23.1 ± 2.1 μg m⁻³) and K⁺ (0.27 ± 0.08 μg m⁻³) were obtained whereas elevated
284 concentrations of levoglucosan (119.6 ± 6.0 ng m⁻³), K⁺ (0.33 ± 0.07 μg m⁻³), and OC
285 (10.8 ± 1.1 μg m⁻³) were measured during the Siberia forest fire episode. As shown in
286 Fig. 9, a similar level of OC was observed during the entire measurement period except
287 the Siberia forest fire episode. However, several peaks of SO₄²⁻ concentrations were
288 observed with the highest peak during the Chinese haze episode.

289 Figure 10 shows PM_{2.5} mass closures during the Chinese haze and Siberia forest fire
290 episodes. Concentrations of organic aerosols (OM) were reconstructed from measured
291 OC concentrations by multiplying the OM/OC ratio of 1.8 that was measured by an
292 aerosol mass spectrometer in Korea during spring to fall, 2011 under the Asian
293 continental outflow (personal communication from prof. T. Lee). Huang et al. (2011)
294 also reported a similar OM/OC ratio of 1.77 ± 0.08 measured at the downwind site of
295 the highly polluted Pearl River Delta cities in China during the fall, 2008. During the
296 Chinese haze episode, SO₄²⁻ was found as the most dominant species in PM_{2.5} mass
297 with an average contribution of 44.2%, followed by organic aerosols (16.6%) and
298 NH₄⁺ (19.1%). This result implies that the Chinese haze episode was mainly attributed
299 to anthropogenic pollutants, possibly emissions from industrial complexes and urban
300 cities in the East China. However, during the Siberia forest fire episode, organic
301 aerosol was the most dominant species in PM_{2.5} mass with an average contribution of
302 38.6%, followed by SO₄²⁻ (16.5%) and NH₄⁺ (10.0%). The high concentration of



303 organic aerosols indicated that the Siberia forest fire episode was mainly originated
304 from biomass burning.

305

306 3.3.2 Comparison of biomass burning tracers between two haze episodes in the Daejeon
307 atmosphere

308 Levoglucosan, mannosan, and K^+ are widely used as an indicator of biomass
309 burning. Levoglucosan and mannosan are formed during pyrolysis of cellulose and
310 hemicellulose, and are not emitted from burning of other materials, such as fossil fuels
311 (Simoneit et al., 1999; Caseiro et al., 2009; Elias et al., 2001). However, caution is
312 required when K^+ is used as a biomass-burning tracer because K^+ can also be emitted
313 from sea salt and soil (Pio et al., 2008). The mass concentrations of biomass burning
314 tracers and their ratios during the Siberia forest fire and Chinese haze episodes are
315 summarized in Table 1 and 2.

316 Significantly elevated concentrations of levoglucosan were observed during the
317 Siberia forest fire episode whereas relatively much less increases in concentration of
318 levoglucosan were observed during the Chinese haze episode in Fig. 9. Concentrations
319 of levoglucosan during the Siberia forest fire episode were measured to be 119.6 ± 6.0
320 ng m^{-3} , approximately 6 times higher than those during the Chinese haze episode (22.3
321 $\pm 11.8 \text{ ng m}^{-3}$) as shown in Table 1. On the other hand, similar levels of K^+ were
322 obtained during the Chinese haze ($0.27 \pm 0.08 \mu\text{g m}^{-3}$) and Siberia forest fire ($0.33 \pm$
323 $0.07 \mu\text{g m}^{-3}$) episodes. Thus, relatively high levoglucosan/ K^+ ratios were obtained
324 during the Siberia forest fire episode (0.37 ± 0.06) compared to those (0.08 ± 0.03)
325 during the Chinese haze episode (Table 2). However, similar levels of
326 levoglucosan/mannosan ratio were estimated as an average of 3.43 ± 0.11 during the



327 Siberia forest fire episode compared to those during the Chinese haze episodes ($4.81 \pm$
328 0.41) as shown in Table 2.

329 Positive correlation was obtained between levoglucosan and OC concentrations
330 during the Siberia forest fire and Chinese haze episodes in Fig. 11a. OC concentrations
331 increased simultaneously as K^+ concentrations increased during the Siberia forest fire
332 episode. However, during the Chinese haze episode, relatively small increase in OC
333 concentrations was observed even though K^+ concentrations increased (Fig. 11b). Much
334 higher OC/EC ratios were obtained during the Siberia forest fire episode (7.18 ± 0.2)
335 compared to those (2.4 ± 0.4) during the Chinese haze episode (Table 1).

336 Good correlations of K^+ concentration with OC and levoglucosan concentrations
337 during the Siberia forest fire episode suggest that K^+ was mainly originated from the
338 smoke plume during the Siberia forest fire episode. However, different correlation
339 patterns between K^+ with levoglucosan and OC concentrations were observed during
340 the Chinese haze episode. This different correlation pattern can be explained as follows.
341 First, different type of biomass burning might occur during the Chinese haze episode
342 compared the Siberia forest fire episode. It can be postulated that biomass burning
343 emissions with relatively lower OC/ K^+ and levoglucosan/ K^+ ratio might impact on the
344 Korean Peninsula during the Chinese haze episode.

345 Second, K^+ during the Chinese haze episode might be originated from other sources
346 rather than biomass burning. Because OC is predominantly emitted from biomass
347 burnings, biomass burning particles have relatively high OC/EC ratio and have good
348 correlation with biomass burning tracers (Cao et al., 2008; Cheng et al., 2008;
349 Popovicheva et al., 2014). Poor correlations of K^+ with OC and levoglucosan
350 concentrations during the Chinese haze episode suggest that the elevated K^+



351 concentration might be due to emissions from other sources such as soil and sea salt or
352 industrial complexes. Chow et al. (2008) reported that 3.9%–12.5% of $PM_{2.5}$ consisted
353 of K^+ in stack samples from cement kiln manufacturing process. Positive correlations of
354 K^+ with SO_4^{2-} and EC concentrations in Fig. 9 during the Chinese haze episode also
355 support that there were additional emission of K^+ from anthropogenic sources except
356 biomass burning.

357 Elevated concentrations of levoglucosan and OC and relatively high OC/EC ratio
358 (7.18 ± 0.2) support that the haze episode occurred during the late July, 2014 was
359 mainly caused by the long-range transported smoke emitted from the Siberia forest fires.
360 However, significantly elevated SO_4^{2-} concentration with relatively weak increases in
361 OC and levoglucosan concentrations and relatively lower OC/EC ratio implies that the
362 Chinese haze episode was mainly caused by anthropogenic pollutants emitted from
363 industrial complexes and urban cities in the East China with relatively little contribution
364 of biomass burning.

365

366 3.3.3 Tracking major sources of biomass burning during the Siberia forest fire episode

367 Levoglucosan to mannosan ratios (Levo/Man ratio) and levoglucosan to K^+ ratios
368 (Levo/ K^+ ratio) during the Siberia forest fire episode are compared with those from
369 previous chamber and ambient studies in Fig. 12. Hardwood burnings have relatively
370 higher Levo/Man ratios with a mean value of 28 (range: 2.2–195) (Fine et al., 2001,
371 2002, 2004a, 2004b; Schauer et al., 2001; Engling et al., 2006; Schmidl et al., 2008a;
372 Bari et al., 2009; Gonçalves et al., 2010) whereas softwood burning have relatively
373 lower Levo/Man ratios (mean: 4.3, range: 2.5–6.7) (Fine et al., 2001, 2002, 2004a,



374 2004b; Schauer et al., 2001; Hays et al., 2002; Engling et al., 2006; Iinuma et al., 2007;
375 Schmidl et al., 2008a; Gonçalves et al., 2010). Grass (mean: 18, range: 9.2-39) and crop
376 residue burnings (mean: 29, range: 12–55) have relatively high Levo/Man ratios
377 compared to leaf burnings (mean: 5.6, range: 5.1–6.0) (Sheesley et al., 2003; ; Engling
378 et al., 2006, 2009; Sullivan et al., 2008; Schmidl et al., 2008b; Oanh et al., 2011; Cheng
379 et al., 2013). Levo/Man ratios (mean: 5.3) during the smoke episode in Moscow,
380 Russian during summer, 2010 are similar to those from softwood and leaf burnings
381 (Popovicheva et al., 2014).

382 Because levoglucosan and mannosan are emitted from similar burning processes,
383 Levo/Man ratio can be used as an indicator to track type of biomass burning. Levo/Man
384 ratios during the Siberia forest fire episode are similar to those obtained from the
385 softwood and leaf burning experiments and the smoke episode in Moscow, Russia
386 during summer, 2010. However, Levo/Man ratios during the Siberia forest fire episode
387 are much lower than those from the hardwood, grass and crop residue burnings.

388 Hardwood and softwood burnings have relatively high Levo/K⁺ ratios, with mean
389 values of 26 and 46, and ranges of 2.2–195 and 4.6–261, respectively (Fine et al., 2001,
390 2002, 2004a, 2004b; Schauer et al., 2001; Hays et al., 2002; Engling et al., 2006; Iinuma
391 et al., 2007; Schmidl et al., 2008a; Bari et al., 2009; Gonçalves et al., 2010). However,
392 grass, crop residue, and leaf burnings have relatively low Levo/K⁺ ratios, with mean
393 values of 3.3, 0.53, and 2.9 and ranges of 0.06–9.5, 0.1–1.2, and 2.4–3.4, respectively
394 (Sheesley et al., 2003; Engling et al., 2006, 2009; Sullivan et al., 2008; Schmidl et al.,
395 2008b; Oanh et al., 2011; Cheng et al., 2013). Levo/K⁺ ratios (mean: 2.8) during the
396 smoke episode in Moscow, Russian during summer 2010 are similar those from grass,



397 crop residue, and leaf burnings (Popovicheva et al., 2014).

398 Levo/K⁺ ratio during the Siberia forest fire episode is close to those from the grass,
399 crop residue, leaf burnings and the smoke episode in Moscow but much lower than
400 those from the hardwood and softwood burnings as shown in Fig. 12b. Levoglucosan
401 can be removed through photo-oxidative decay during the atmospheric transport
402 (Hennigan et al., 2010) but K⁺ is relatively stable in the atmosphere. Laboratory
403 chamber experiments show that levoglucosan decays as a function of integrated OH
404 exposure with a typical lifetime of 0.7–2.2 days (Hennigan et al., 2010). Thus, Levo/K⁺
405 ratios can decrease during the long-range atmospheric transport. Relatively lower
406 Levo/K⁺ ratio during the Siberia forest fire episode was observed compared to those
407 during the smoke episode in Moscow, Russia during summer, 2010, which can be
408 explained by photochemical degradation of levoglucosan during the long-range
409 atmospheric transport.

410 Based on the comparison of biomass burning tracers from various sources in Fig.
411 12, it is suggested that smoke aerosols during the Siberia forest fire episode was mainly
412 originated from the burning of forest leaf in the Siberia region and their long-range
413 atmospheric transport. Smoke aerosols during the smoke episode in Moscow, Russia
414 during the summer, 2010 have very similar Levo/Man and Levo/K⁺ ratios with those
415 from the leaf burning in Fig. 12. These also support that the smoke episode in the
416 Russian forest is mainly originated from burnings of forest leaf.

417

418 4. Conclusion

419 This study investigated long-range transported smoke plumes emitted from the
420 Siberia forest fires occurred during the late July, 2014. Smoke plumes emitted from



421 Siberia forest fires are generally transported to the Northwest Pacific due to the
422 prevailing westerlies. However, the haze plume occurred during the late July, 2014 had
423 a significant impact on the Korean Peninsula located at ~3,000 km south of the Siberia
424 forest. From spatial distributions of AOD obtained by MODIS satellite, CALIPSO
425 satellite observation, and HYSPLIT air mass backward trajectory analyses, it was
426 clearly seen that the smoke plumes originated from the Siberia forest fires during 23–24
427 July 2014 transported over 3,000 km to south direction and had an impact on the
428 Korean Peninsula during 27–28 July 2014. During that episodic period, elevated
429 concentrations of levoglucosan ($119.6 \pm 6.0 \text{ ng m}^{-3}$) and K^+ ($0.33 \pm 0.07 \text{ } \mu\text{g m}^{-3}$) with
430 high OC/EC ratio (7.18 ± 0.2) were observed at the measurement site in Daejeon, Korea.
431 These results support that the haze episode occurred during the late July, 2014 was
432 mainly caused by the long-range transport of the smoke plume emitted from Siberia
433 forest fires. The Siberia smoke episode clearly distinguished compared to the haze
434 episode caused by long-range transported anthropogenic pollutants emitted from the
435 East China which showed elevated SO_4^{2-} concentration with weak increases in OC and
436 levoglucosan concentrations.

437

438 Acknowledgement

439 This work was conducted by a co-research project of National Institute of
440 Environmental Research (NIER) and Korea Research Institute of Standards and Science
441 (KRISS). This work was funded by the National Research Foundation under grant NRF-
442 2015R1C1A1A02036580. We thank to Dr. B. Holben and Dr. M. Panchenko for their
443 efforts in establishing and maintaining Yakutsk and Ussuriysk AERONET sites in
444 Russia. The authors gratefully acknowledge the NOAA Air Resources Laboratory (ARL)



445 for the provision of the HYSPLIT transport and dispersion model and/or READY
446 website (<http://www.arl.noaa.gov/ready.html>) used in this publication. The authors also
447 thank the NASA-US for making available the Collection 005 Level-2 MODIS data.
448
449



450 **Reference**

451

452 Bartalev, S. A., Korovin, G. N., and Shlepak, B. V.: Assessments of Forest Fire
453 Recognition, Using the NOAA AVHRR Radiometers, in: Proceedings of
454 International Forum on Problems in Science, Technology and Education, Vol. II,
455 Moscow, 22–25, 1977.

456 Bari, M. A., Baumbach, G., Kuch, B., and Scheffknecht, G.: Wood smoke as a source of
457 particle-phase organic compounds in residential areas, *Atmos. Environ.*, 43, 4722–
458 4732, 2009.

459 Birch, M. E., and Cary, R. A.: Elemental carbon-based method for monitoring
460 occupational exposure to particulate diesel exhaust, *Aerosol Sci. Tech.*, 25, 221–
461 241, 1996.

462 Bondur, V. G.: Importance of aerospace remote sensing approach to the monitoring of
463 nature fire in Russia, *International Forest Fire News (IFFN)*, (40), 43–57, 2010.

464 Cao, G., Zhang, X., Gong, S., and Zheng, F.: Investigation on emission factors of
465 particulate matter and gaseous pollutants from crop residue burning, *J. Environ.*
466 *Sci.*, 20, 50–55, 2008.

467 Carvalho, A., Monteiro, A., Flannigan, M., Solman, S., Miranda, A. I., and Borrego, C.:
468 Forest fires in a changing climate and their impacts on air quality, *Atmos. Environ.*,
469 45, 5545–5553, 2011.

470 Caseiro, A., Bauer, H., Schmidl, C., Pio, C. A., and Puxbaum, H.: Wood burning impact
471 on PM₁₀ in three Austrian regions, *Atmospheric Environment*, 43, 2186–2195, 2009.

472 Chan, C. K., and Yao, X.: Air pollution in mega cities in China, *Atmos. Environ.*, 42, 1–
473 42, 2008.

474 Cheng, M. T., Horng, C. L., Su, Y. R., Lin, L. K., Lin, Y. C., and Chou, C. K.:
475 Particulate matter characteristics during agricultural waste burning in Taichung City,
476 Taiwan, *J. Hazard. Mater.*, 165, 187–192, 2008.

477 Cheng, Y., Engling, G., He, K. B., Duan, F. K., Ma, Y. L., Du, Z. Y., Liu, J. M., Zheng,
478 M., and Weber, R. J.: Biomass burning contribution to Beijing aerosol, *Atmos.*
479 *Chem. Phys.*, 13, 7765–7781, 2013.

480 Chow, J. C., Watson, J. G., Kuhns, H., Etyemezian, V., Lowenthal, D. H., Crow, D.,



- 481 Kohl, S. D., Engelbrecht, J. P., and Green, M. C.: Source profiles for industrial,
482 mobile, and area sources in the Big Bend Regional Aerosol Visibility and
483 Observational study, *Chemosphere*, 54, 185–208, 2004.
- 484 Conard, S. G., and Ivanova, G. A.: A Differential Approach to Numerical Assessment of
485 Forest Fire Carbon Emissions, *Lesovedenie (Forestry)*, 3, 28–35, 1988.
- 486 Crutzen, P., Heidt, L., Krasnec, J., Pollock, W., and Seiler, W.: Biomass burning as a
487 source of atmospheric gases CO, H₂, N₂O, NO, CH₃Cl and COS, *Nature*, 282
488 (5736), 253–256, 1979.
- 489 Elias, V. O., Simoneit, B. R. T., Cordeiro, R. C., and Turcq, B.: Evaluating levoglucosan
490 as an indicator of biomass burning in Carajás, Amazônia: a comparison to the
491 charcoal record, *Geochim. Cosmochim. Acta*, 65, 267–272, 2001.
- 492 Engling, G., Carrico, C.M., Kreidenweis, S. M., Collett Jr, J. L., Day, D. E., Malm, W.
493 C., Lincoln, L., Hao, W. M., Iinuma, Y., and Herrmann, H.: Determination of
494 levoglucosan in biomass combustion aerosol by high-performance anion-exchange
495 chromatography with pulsed amperometric detection, *Atmos. Environ.*, 40, S299–
496 S311, 2006.
- 497 Engling, G., Lee, J. J., Tsai, Y. W., Lung, S. C. C., Chou, C. C. K., and Chan, C. Y.:
498 Size-resolved anhydrosugar composition in smoke aerosol from controlled field
499 burning of rice straw, *Aerosol Sci. Tech.*, 43, 662–672, 2009.
- 500 Fine, P. M., Cass, G. R., and Simoneit, B. R. T.: Chemical characterization of fine
501 particle emissions from fireplace combustion of woods grown in the northeastern
502 United States, *Environ. Sci. Tech.*, 35, 2665–2675, 2001.
- 503 Fine, P. M., Cass, G. R., and Simoneit, B. R. T.: Chemical characterization of fine
504 particle emissions from the fireplace combustion of woods grown in the southern
505 United States, *Environ. Sci. Tech.*, 36, 1442–1451, 2002.
- 506 Fine, P. M., Cass, G. R., and Simoneit, B. R. T.: Chemical characterization of fine
507 particle emissions from the fireplace combustion of wood types grown in the
508 midwestern and western United States, *Environ. Eng. Sci.*, 21, 387–409, 2004a.
- 509 Fine, P. M., Cass, G. R., and Simoneit, B. R. T.: Chemical characterization of fine
510 particle emissions from the wood stove combustion of prevalent United States tree
511 species, *Environ. Eng. Sci.*, 21, 705–721, 2004b.
- 512 Giglio, L., Descloitres, J., Justice, C. O., and Kaufman, Y. J.: An enhanced contextual



- 513 fire detection algorithm for MODIS, *Remote Sens. Environ.*, 87(2–3), 273–282,
514 2003.
- 515 Gonçalves, C., Alves, C., Evtyugina, M., Mirante, F., Pio, C., Caseiro, A., Schmidl, C.,
516 Bauer, H., and Carvalho, F.: Characterisation of PM₁₀ emissions from wood stove
517 combustion of common woods grown in Portugal, *Atmos. Environ.*, 44, 4474–4480,
518 2010.
- 519 Hays, M. D., Geron, C. D., Linna, K. J., Smith, N. D., and Schauer, J. J.: Speciation of
520 gas-phase and fine particle emissions from burning of foliar fuels, *Environ. Sci.*
521 *Tech.*, 36, 2281–2295, 2002.
- 522 Hennigan, C. J., Sullivan, A. P., Collett Jr, J. L., and Robinson, A. L.: Levoglucosan
523 stability in biomass burning particles exposed to hydroxyl radicals, *Geophys. Res.*
524 *Lett.*, 37, doi:10.1029/2010GL043088, 2010.
- 525 Huang, X. F., He, L., Hu, M., Cengaratna, M. R., Kroll, J. H., Ng, N. L., Zhang, Y. H.,
526 Lin, Y., Xue, L., Sun, T. L., Liu, X. G., Shao, M., Jayne, J. T., and Worsnop, D. R.:
527 Characterization of submicron aerosols at a rural site in Pearl River Delta of China
528 using an Aerodyne High-Resolution Aerosol Mass Spectrometer, *Atmos. Chem.*
529 *Phys.*, 11, 1865–1877, 2011.
- 530 Iinuma, Y., Brüggemann, E., Gnauk, T., Müller, K., Andreae, M. O., Helas, G., Parmar,
531 R., and Herrmann, H.: Source characterization of biomass burning particles: The
532 combustion of selected European conifers, African hardwood, savanna grass, and
533 German and Indonesian peat, *J. Geophys. Res.*, 112, D08209,
534 doi:10.1029/2006JD007120, 2007.
- 535 Isaev, A. S., Korovin, G. N., Bartalev, S. A., Ershov, D. V., Janetos, A., Kasischke, E. S.,
536 Shugart, H. H., French, N. H. F., Orlick, B. E., and Murphy, T. L.: Using Remote
537 Sensing to Assess Russian Forest Fire Carbon Emissions, *Climatic Change*, 55,
538 235–249, 2002.
- 539 Jeong, H., Chung, C. E., van Noije, T., and Takemura, T.: Relationship between fine-
540 mode AOD and precipitation on seasonal and interannual time scales, *Tellus Ser. B*,
541 66, 23037, doi:10.3402/tellusb.v66.23037, 2014.
- 542 Jeong, J. I., Park, R. J., and Youn, D.: Effects of Siberian forest fires on air quality in
543 East Asia during May 2003 and its climate implication, *Atmos. Environ.*, 42, 8910–
544 8922. doi:10.1016/j.atmosenv.2008.08.037, 2008.



- 545 Kajii, Y., Kato, S., Streets, D. G., Tsai, N. Y., Shvidenko, A., Nilsson, S., Minko, N. P.,
546 Abushenko, N., Altyntsev, D., and Khodzer, T. V.: Boreal forest fires in Siberia in
547 1998: estimation of area and emissions of pollutants by AVHRR satellite data, *J.*
548 *Geophys. Res.*, 107 (D24), 4745, 2002.
- 549 Kanaya, Y., Kajii, Y., and Akimoto, H.: Solar actinic flux and photolysis frequency
550 determinations by radiometers and a radiative transfer model at Rishiri Island:
551 comparisons, cloud effects, and detection of an aerosol plume from Russian forest
552 fires, *Atmos. Environ.*, 37 (18), 2463–2475, 2003.
- 553 Lee, K. H., Kim, J. E., Kim, Y. J., Kim, J., and Von Hoyningen-Huene, W.: Impact of
554 the smoke aerosol from Russian forest fires on the atmospheric environment over
555 Korea during May 2003, *Atmos. Environ.*, 39, 85–99, 2005.
- 556 Li, L., An, J. Y., Zhou, M., Yan, R. S., Huang, C., Lu, Q., Lin, L., Wang, Y. J., Tao, S. K.,
557 Qiao, L. P., Zhu, S. H., and Chen, C. H.: Source apportionment of fine particles and
558 its chemical components over the Yangtze River Delta, China during a heavy haze
559 pollution episode, *Atmos. Environ.*,
560 <http://dx.doi.org/10.1016/j.atmosenv.2015.06.051>, 2015(in press).
- 561 Mei, L., Xue, Y., de Leeuw, G., Guang, J., Wang, Y., Li, Y., Xu, H., Yang, L., Hou, T.,
562 He, X., Wu, C., Dong, J., and Chen, Z.: Integration of remote sensing data and
563 surface observations to estimate the impact of the Russian wildfires over Europe
564 and Asia during August 2010, *Biogeosciences*, 8, 3771–3791, 2011.
- 565 Oanh, N. T. K., Ly, B. T., Tipayarom, D., Manandhar, B. R., Prapat, P., Simpson, C. D.,
566 and Liu, L. J. S.: Characterization of particulate matter emission from open burning
567 of rice straw, *Atmos. Environ.*, 45, 493–502, 2011.
- 568 Pio, C. A., Legrand, M., Alves, C. A., Oliveira, T., Afonso, J., Caseiro, A., Puxbaum, H.,
569 Sanchez-Ochoa, A., and Gelencsér, A.: Chemical composition of atmospheric
570 aerosols during the 2003 summer intense forest fire period, *Atmos. Environ.*, 42,
571 7530–7543, 2008.
- 572 Popovicheva, O., Kistler, M., Kireeva, E., Persiantseva, N., Timofeev, M., Kopeikin, V.,
573 and Kasper-Giebl, A.: Physicochemical characterization of smoke aerosol during
574 large-scale wildfires: Extreme event of August 2010 in Moscow, *Atmos. Environ.*,
575 96, 405–414, 2014.



- 576 Quennehen, B., Schwarzenboeck, A., Matsuki, A., Burkhart, J. F., Stohl, A., Ancellet, G.,
577 and Law, K. S.: Anthropogenic and forest fire pollution aerosol transported to the
578 Arctic: observations from the POLARCAT-France spring campaign, *Atmos. Chem.*
579 *Phys.*, 12, 6437–6454, 2012.
- 580 Schauer, J. J., Kleeman, M. J., Cass, G. R., and Simoneit, B. R. T.: Measurement of
581 emissions from air pollution sources. 3. C1-C29 organic compounds from fireplace
582 combustion of wood, *Environ. Sci. Tech.*, 35, 1716–1728, 2001.
- 583 Schmidl, C., Marr, I. L., Caseiro, A., Kotianová, P., Berner, A., Bauer, H., Kasper-Giebl,
584 A., and Puxbaum, H.: Chemical characterisation of fine particle emissions from
585 wood stove combustion of common woods growing in mid-European Alpine
586 regions, *Atmos. Environ.*, 42, 126–141, 2008a.
- 587 Schmidl, C., Bauer, H., Dattler, A., Hitzenberger, R., Weissenboeck, G., Marr, I. L., and
588 Puxbaum, H.: Chemical characterisation of particle emissions from burning leaves,
589 *Atmos. Environ.*, 42, 9070–9079, 2008b.
- 590 Schreier, S. F., Richter, A., Schepaschenko, D., Shvidenko, A., Hilboll, A., and Burrows,
591 J.P.: Differences in satellite-derived NO_x emission factors between Eurasian and
592 North American boreal forest fires, *Atmos. Environ.*, 121, 55–65, 2015.
- 593 Sheesley, R. J., Schauer, J. J., Chowdhury, Z., Cass, G. R., and Simoneit, B. R. T.:
594 Characterization of organic aerosols emitted from the combustion of biomass
595 indigenous to South Asia, *J. Geophys. Res.*, 108, 4285, doi:10.1029/2002JD002981,
596 2003.
- 597 Simoneit, B. R. T., Schauer, J. J., Nolte, C. G., Oros, D. R., Elias, V. O., Fraser, M. P.,
598 Rogge, W. F., and Cass, G. R.: Levoglucosan, a tracer for cellulose in biomass
599 burning and atmospheric particles, *Atmos. Environ.*, 33, 173–182, 1999.
- 600 Stohl, A.: Computation, accuracy and applications of trajectories: A review and
601 bibliography, *Atmos. Environ.*, 32, 947–966, 1998.
- 602 Sullivan, A. P., Holden, A. S., Patterson, L. A., McMeeking, G. R., Kreidenweis, S. M.,
603 Malm, W. C., Hao, W. M., Wold, C. E., and Collett Jr., J. L.: A method for smoke
604 marker measurements and its potential application for determining the contribution
605 of biomass burning from wildfires and prescribed fires to ambient $\text{PM}_{2.5}$ organic
606 carbon, *J. Geophys. Res.*, 113, D22302, doi:10.1029/2008JD010216, 2008.
- 607 Youn, D., Park, R. J., Jeong, J. I., Moon, B. K., Yeh, S. W., Kim, Y. H., Woo, J. H., Im,



608 E. G., Jeong, J. H., Lee, S. J., and Song, C. K.: Impacts of aerosols on regional
609 meteorology due to Siberian forest fires in May 2003, Atmos. Environ., 45, 1407–
610 1412, 2011.



Table 1. Summary of fine particle (PM_{2.5}) mass, organic and inorganic chemical composition of PM_{2.5} particles during the Chinese haze and Siberian forest fire episodes measured at Daejeon in Korea during summer, 2014.

Components	Unit	¹ Chinese Haze	² Siberia Forest Fire
		Range (Average ± 1σ)	
PM _{2.5} mass		44.5–65.1 (52.3 ± 11.1)	44.3–56.2 (50.2 ± 8.4)
SO ₄ ²⁻		20.9–25.1 (23.1 ± 2.1)	7.4–9.2 (8.3 ± 1.3)
NO ₃ ⁻		0.9–5.0 (2.8 ± 2.1)	1.1–1.7 (1.4 ± 0.4)
NH ₄ ⁺	(μg m ⁻³)	6.1–12.7 (10.0 ± 3.5)	4.6–5.4 (5.0 ± 0.6)
OC		3.6–5.7 (4.8 ± 1.1)	10.0–11.6 (10.8 ± 1.1)
EC		1.9–2.2 (2.0 ± 0.2)	1.4–1.6 (1.5 ± 0.2)
K ⁺		0.17–0.33 (0.27 ± 0.08)	0.28–0.38 (0.33 ± 0.07)
OC/EC ratio		1.93–2.64 (2.4 ± 0.41)	7.04–7.32 (7.18 ± 0.19)
Levoglucosan		13.4–35.7 (22.3 ± 11.8)	115.4–123.9 (119.6 ± 6.0)
Mannosan	(ng m ⁻³)	3.0–6.8 (4.5 ± 2.0)	32.9–37.0 (34.9 ± 2.9)

¹Chinese haze: during 14–16 July 2014

²Siberia forest fire: during 27–28 July 2014



Table 2. Summary of ratios among biomass burning tracers during the Chinese haze and Siberian forest fire episodes measured at Daejeon in Korea during summer, 2014.

Components	Chinese Haze	Siberia Forest Fire
	Range (Average $\pm 1\sigma$)	
Levogluconan/Mannosan ratio	4.41–5.22 (4.81 \pm 0.41)	3.35–3.51 (3.43 \pm 0.11)
Levogluconan/K ⁺ ratio	0.05–0.11 (0.08 \pm 0.03)	0.33–0.41 (0.37 \pm 0.06)



Figure captions

Fig. 1. Area map of the measurement site (36.19 °N, 127.24 °E) in Daejeon, Korea (@Google Map). Siberia forest is located at ~3,000 km north of the Korean Peninsula.

Fig. 2. Temporal variation of chemical components of fine particulate matter (PM_{2.5}) at the Daejeon site during July, 2014. Daily average PM_{2.5} mass concentrations were obtained from a beta-attenuation technique.

Fig. 3. (a) MODIS RGB image on 25 July 2014 and (b) air mass backward trajectories during 26–28 July 2014 when smoke plume originated from the Siberia forest fires had an impact on the Korean Peninsula. Red, blue, and green in (b) represent air mass backward trajectories arriving at 200 m, 500 m, and 1000 m heights, respectively. The Yakutsk site (61.66 °N, 129.37 °E) and Ussuriysk site (43.70 °N, 132.16 °E) in (b) are AERONET sites in Russia. MODIS RGB image in (a) was obtained from the NASA Worldview website (<https://earthdata.nasa.gov/labs/worldview/>).

Fig. 4. MODIS aerosol optical depth (AOD) over the East Asia from 23 July to 28 July 2014.

Fig. 5. Temporal variations of AOD measured by a sunphotometer at the Yakutsk site and Ussuriysk site, Russia during July 2014.

Fig. 6. MODIS RGB images and vertical profiles of total attenuated backscatter at 532 nm measured by the CALIPSO satellite during (a) 24, (b) 25, and (c) 27 July 2014. Yellow line over MODIS RGB image represents the observation routes of the CALIPSO satellite which is consistent with x-axis in vertical profiles of total



attenuated backscatter images.

Fig. 7. (a) MODIS RGB image during 14 July 2014 and (b) air mass backward trajectories during 15–16 July 2014 when haze plume originated from the East China had an impact on the Korean Peninsula.

Fig. 8. MODIS AOD over the East Asia during 13–15 July 2014.

Fig. 9. Temporal variations of $\text{PM}_{2.5}$ mass, K^+ , levoglucosan, OC, EC and SO_4^{2-} concentrations at the Daejeon site during the entire measurement period.

Fig. 10. Average $\text{PM}_{2.5}$ mass closures during the long-range transported (a) Chinese haze and (b) Siberia forest fires episodes.

Fig. 11. Scatter plots of OC versus (a) levoglucosan and (b) K^+ as well as levoglucosan versus (c) K^+ and (d) mannosan during the entire measurement period. Filled black and red diamonds represent the Chinese haze and Siberia forest fire episodes, respectively.

Fig. 12. (a) Levoglucosan to mannosan ratios and (b) levoglucosan to K^+ ratios obtained from previous chamber studies, extreme smoke episode in Moscow, Russia during summer, 2010, and the Siberia forest fire episode. **Hardwoods:** Fine et al. (2001, 2002, 2004a, 2004b), Schauer et al. (2001), Engling et al. (2006), Schmidl et al. (2008a), Goncalves et al. (2010), Bari et al. (2009); **Softwoods:** Fine et al. (2001, 2002, 2004a, 2004b), Schauer et al. (2001), Engling et al. (2006), Hay et al. (2002), Schmidl et al. (2008a), Goncalves et al. (2010), Iinuma et al. (2007), Cheng et al. (2013); **Grass:** Sullivan et al. (2008); **Crop residue:** Sullivan et al., (2008), Oanh et al. (2011), Sheesley et al. (2003), Engling et al. (2009), Cheng et al. (2013); **Leaf:** Schmidl et al. (2008b); **Moscow smoke:** Popovicheva et al. (2014); **LRT Siberia FF:** This study.





Figure 1





Figure 2

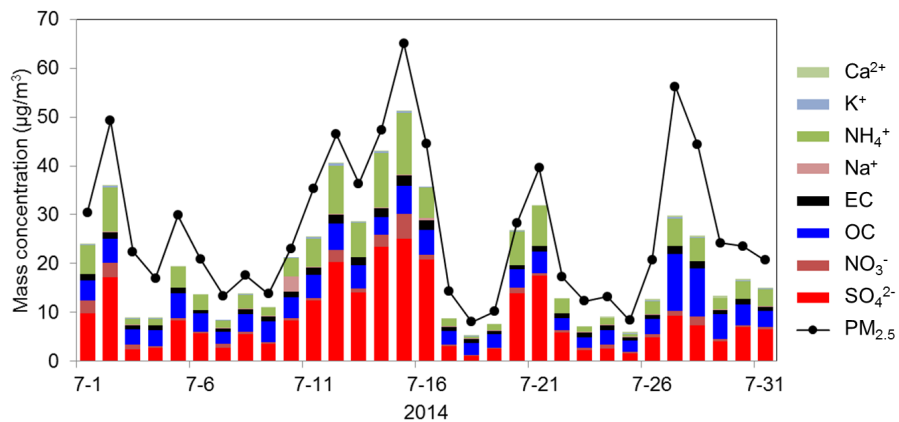




Figure 3

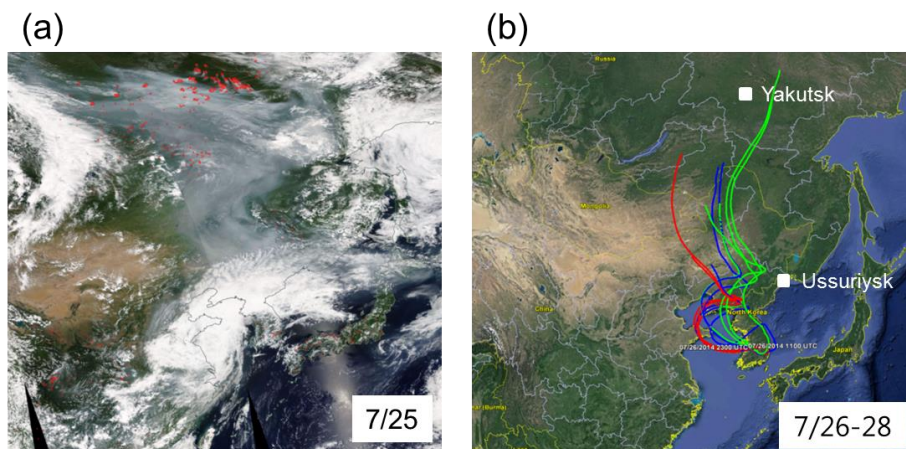




Figure 4

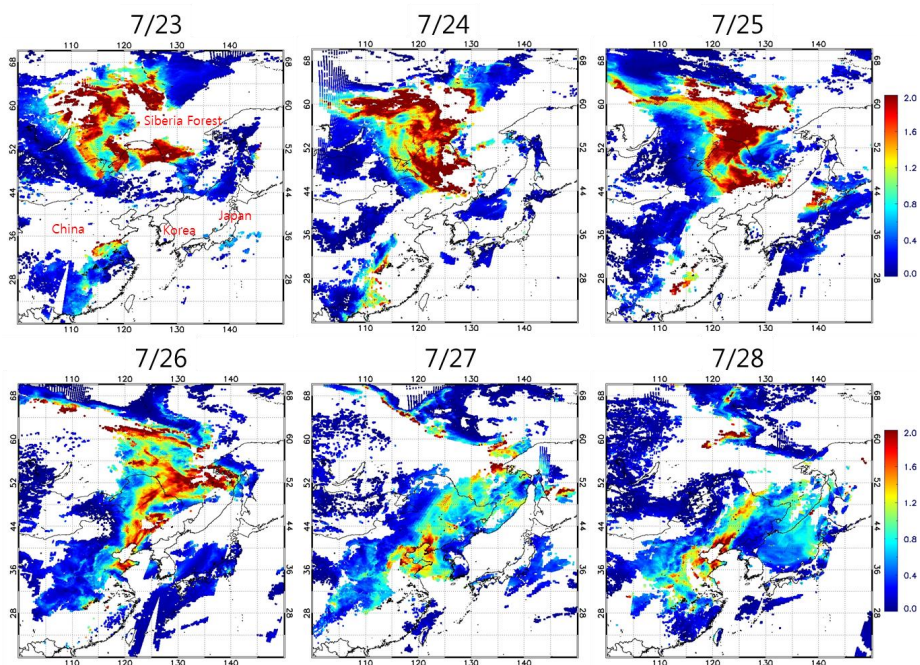




Figure 5

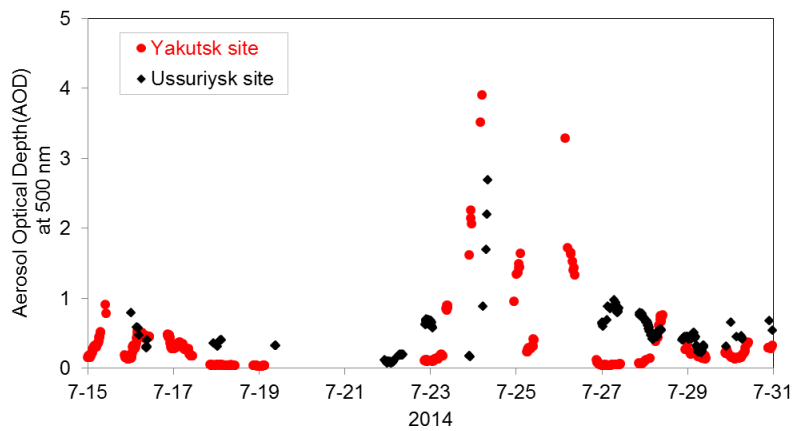




Figure 6

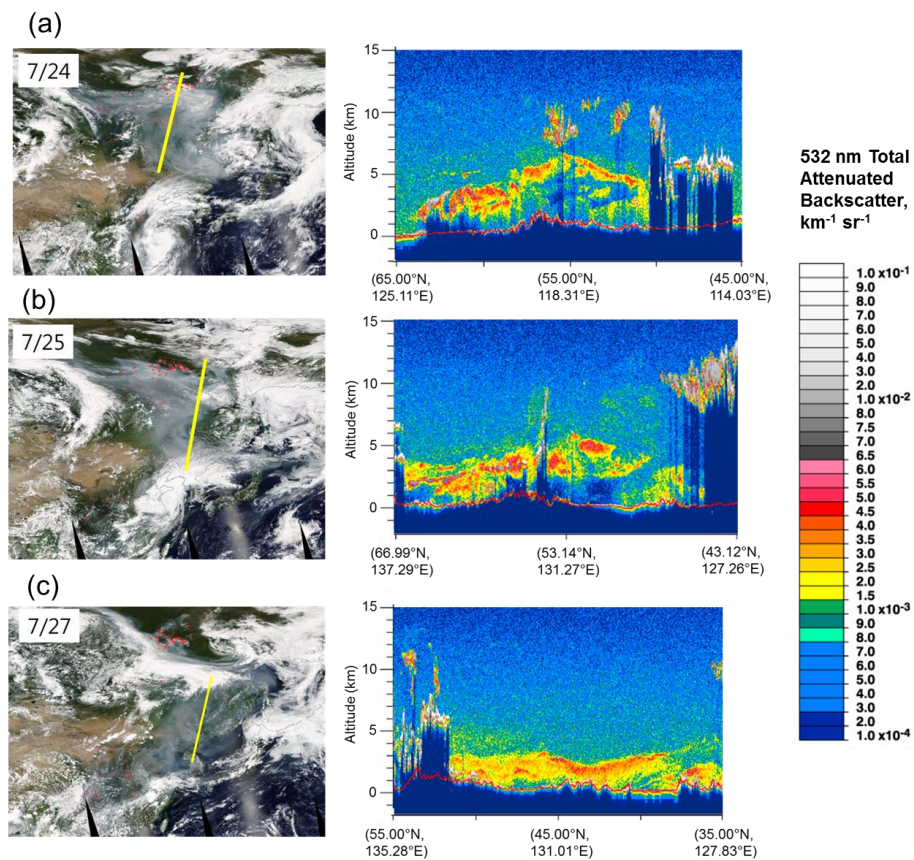




Figure 7

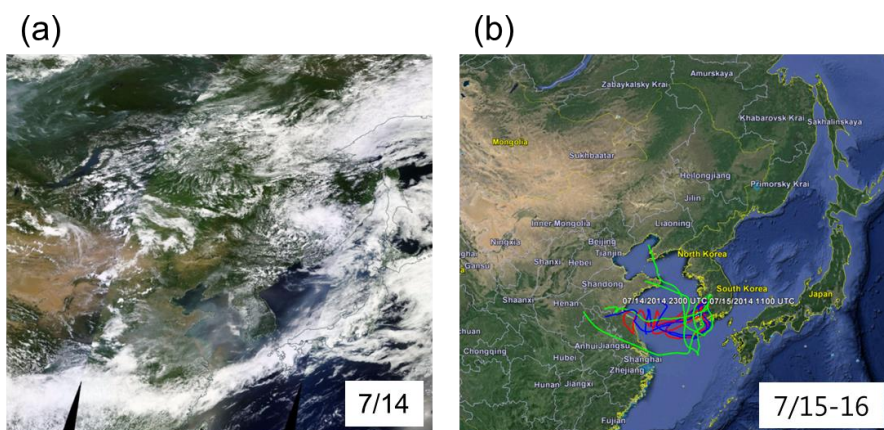




Figure 8

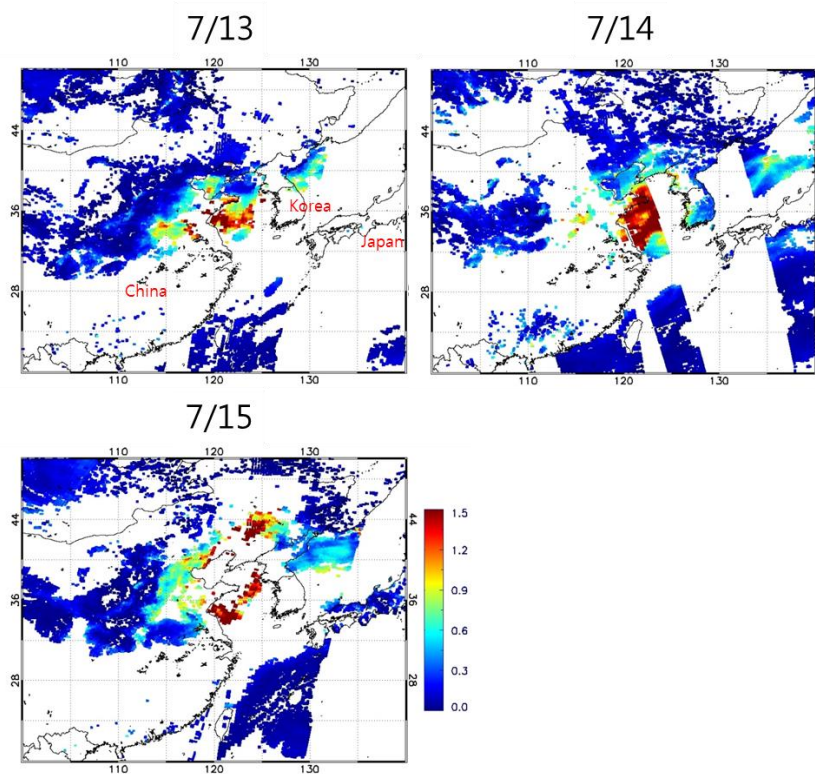




Figure 9

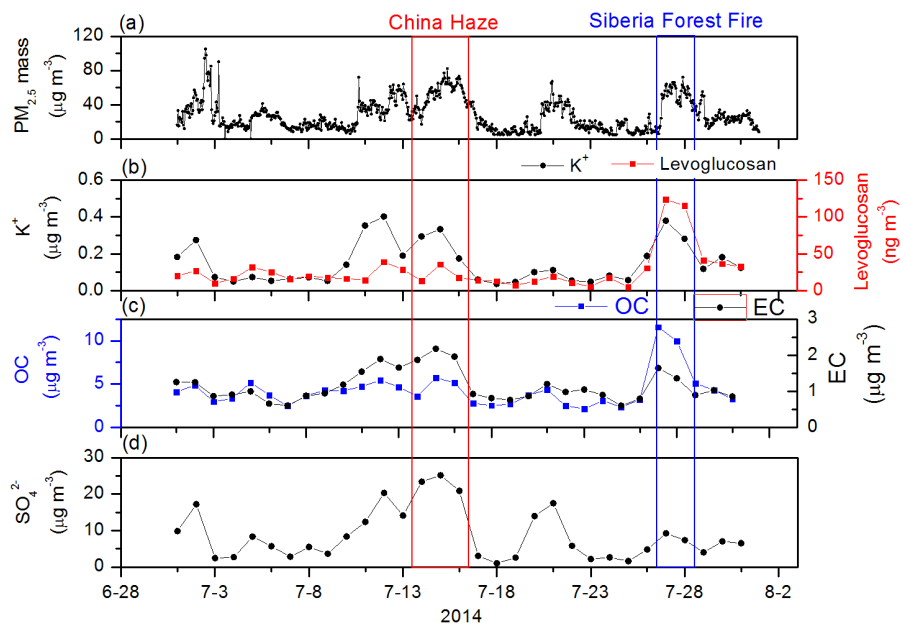




Figure 10

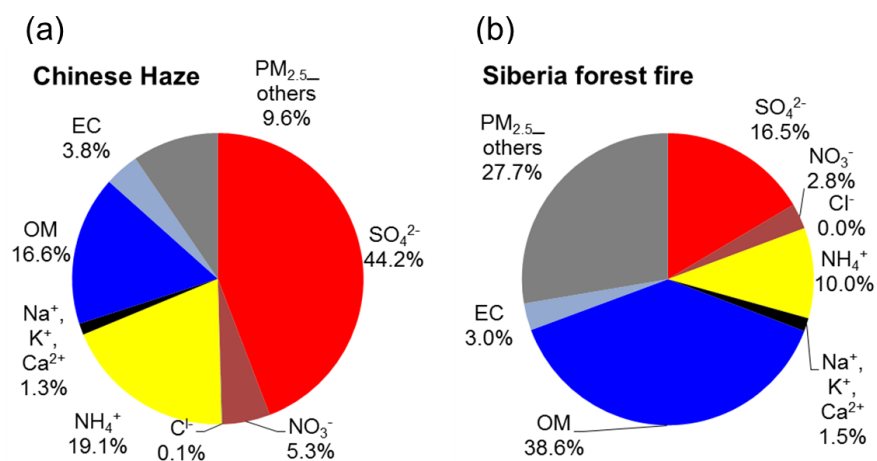




Figure 11

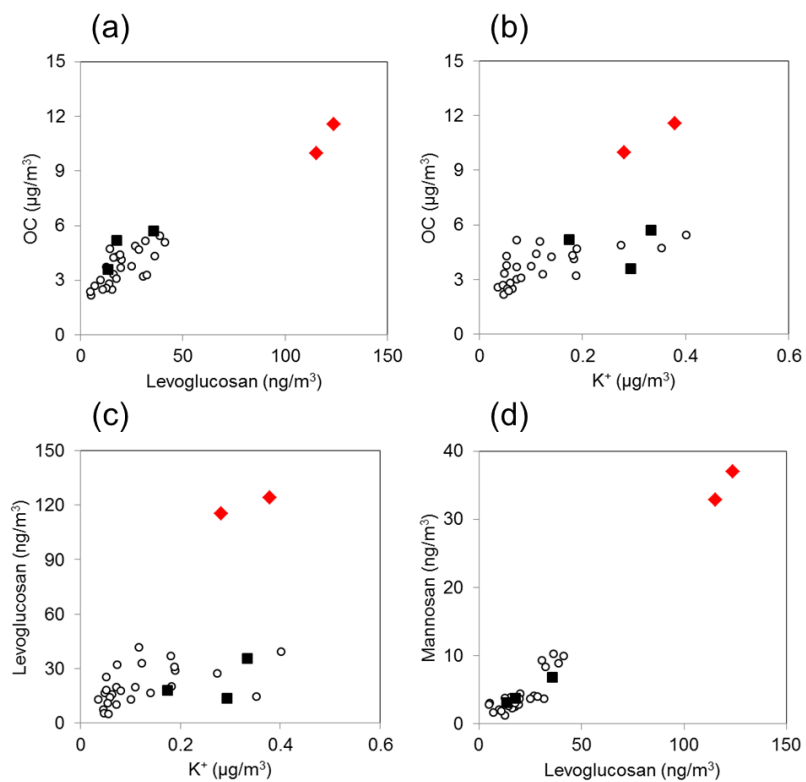




Figure 12

